Preprint Title Structural studies and selected physical investigations of $LiCoO_2$ obtained by combustion synthesis

Authors Monika Michalska, Paweł Ławniczak, Tomasz Strachowski, Adam Ostrowski and Waldemar Bednarski

Publication Date 22 Sep 2022

Article Type Full Research Paper

ORCID® iDs Monika Michalska - https://orcid.org/0000-0002-6120-4950

Structural studies and selected physical investigations of $LiCoO_2$ obtained by combustion synthesis

Monika Michalska*[1,2], Paweł Ławniczak‡[3], Tomasz Strachowski*[2], Adam Ostrowski‡[3] and Waldemar Bednarski‡[3]

Address: [1] Department of Chemistry and Physico-Chemical Processes, Faculty of Materials Science and Technology, VŠB-Technical University of Ostrava, 17. listopadu 15/2172, 708 00 Ostrava-Poruba, Czech Republic

[2] Łukasiewicz Research Network - Institute of Microelectronics and Photonics, Al. Lotników 32/46, 02-668 Warsaw, Poland

[3] Institute of Molecular Physics Polish Academy of Sciences, Smoluchowskiego 17, 60-179 Poznań, Poland

Email: Monika Michalska - michalska.monika83@gmail.com and Tomasz Strachowski – tomasz.strachowski@imif.lukasiewicz.gov.pl

* Corresponding author

‡ Equal contributors

Abstract

The nanocrystalline powders of $LiCoO_2$ were synthesized using a modified solution combustion method and the effects of the annealing temperature (450-900°C) on the structure and composition were investigated using various methods, including XRD, SEM, EPR, and electrical studies. It was found that as the process temperature increases, the value of the specific surface area decreases, and hence the size of the

crystallites increases. XRD analysis showed that the phase pure $LiCoO_2$ material was maintained without additional phases. The EPR studies revealed the presence of two Ni^{3+} complexes. The electrical properties of the studied $LiCoO_2$ samples were investigated by impedance spectroscopy. Comparison of the effect of annealing temperature on electrical conductivity shows a very interesting behavior. As the annealing temperature increases, the DC conductivity value increases, reaching a maximum temperature of 500°C. However, further increase in the annealing temperature causes a steady decrease in the DC conductivity.

Keywords

Lithium-ion battery, solution combustion synthesis, lithium cobalt oxide, nanocrystalline powder

Introduction

Lithium cobalt oxide ($LiCoO_2$, LCO) of hexagonal structure ($R\bar{3}m$) was first used as cathode material in lithium cells in 1979 by researchers from Oxford University [1]. The cell consisted of LCO, which was used as the cathode, and metallic lithium, which was used as the anode material. In 1985, it was proposed to replace the negative electrode Li metal with carbonaceous material graphite capable of reversibly intercalating lithium ions [2]. The commercialization of lithium-ion cells was achieved in the early 1990s by Sony Corporation and in 1992 by a joint venture company (Asahi Kasai and Toshiba) [2-4]. Almost 90% of commercial LiBs consist of a lithium cobalt oxide cathode and a graphite anode immersed in a lithium-ion conducting electrolyte: 1M lithium hexafluorophosphate $LiPF_6$ in a 1:1 (v/v) mixture of ethylene and dimethyl carbonate (EC:DMC) solvents. Most commercial Li-ion cells are used to power

portable devices, including mobile phones, laptops, and cameras [5-7]. However, due to the global and European Union requirements regarding the protection of the environment, batteries consisting of materials with toxic elements, such as cobalt and nickel compounds, are slowly being phased out of use. They are replaced by other materials that are more environmentally friendly. Furthermore, the limited availability of cobalt compounds is reflected in the high price of the $LiCoO_2$ material.

One of the main advantages of the cobalt-based battery is its high theoretical capacity of 274 mAh/g, the high working potential of 4.0 V vs. Li/Li^+, and high energy density, approximately 500 Wh/kg [5-9]. The total removal of lithium ions from the $LiCoO_2$ structure is prevented by the phase transition from a hexagonal structure to a monoclinic structure, which occurs during cathode charging at a potential of approximately 4.2 V [5-9]. The decrease in capacity (approx. 50%) is observed during the cycling charging-discharging processes, which are caused by the dissolution of cobalt ions in the electrolyte above 4.2 V. Therefore, the practical capacity of the LCO material is approximately 150 mAh/g [5-9]. One of the ways to improve unsatisfactory performances is to obtain: i) a nanosized $LiCoO_2$ material in different forms and shapes using chemical or physical syntheses (see discussion below) or ii) substitution of Co ions with other metal ions: Mg, Al, Fe, Ni, Mn, V [10-22] or iii) surface modification by carbon, metal and oxide coatings [15, 16].

As nanomaterials are preferred for use in energy storage and conversion devices, such as Li-ion batteries, solar cells, solid oxide fuel cells, thermoelectrics, and so on, their unusual and unexpected properties and also unique microstructure (and shape) such as high porosity, high surface area, short reaction pathways, and diffusion length for Li-ion transport, finally improving electrical conductivity and electrochemical performances [5-7, 9, 13-16, 23-32]. Nanostructured materials can reduce the specific surface current rate, improve stability, and specific capacity [23-29].

As mentioned above, $LiCoO_2$ has been produced in the form of powders, fibers, and films by using various processing techniques including wet chemical syntheses, such as the sol-gel method [33-35], precipitation [36], hydrothermal [37-39], spray pyrolysis [40, 41] and solid-state syntheses such as mechanical synthesis [42], thermal decomposition [43] or microwave syntheses [44-47].

Wet chemical synthesis allows molecular-level mixing of the starting components, resulting in a very homogeneous product comprising fine particles and a large surface area. The stoichiometry of the product created using wet techniques may be controlled with a greater precision than that of the solid-state method. Combustion synthesis (CS), also known as self-propagating high-temperature synthesis (SHS), is a low-cost process for handling a wide variety of industrially relevant materials. CS is a widely used method for the creation of nanomaterials [48-57]. Acetates, carbonates, and nitrate salts of lithium and cobalt are often utilized as oxidizers in the combustion synthesis of lithium cobalt oxide as starting materials [50, 58-59]. Different ammonium carboxylates were investigated as fuels, including ammonium acetate, ammonium citrate, or ammonium tartarate [55], urea [56], starch [57], citric acid [58] and 1,2-diformylhydrazine [59]. The obtained LCO precursors were annealed in air from 300 to 850°C [55-59].

Herein, wet demonstrated a new combustion solution synthesis (CSS) to obtain a single-phase nanocrystalline lithium cobalt oxide ($LiCoO_2$, LCO) of the layered structure. The dependence between the heating temperature and: 1) structural parameters using XRD analysis (crystallite sizes, lattice parameters, and volume cells), 2) morphologies by SEM (size and distribution of grains), 3) specific surface area SSA using BET measurements, 4) EPR studies and 5) electrical parameters using IS (thermal dependencies of conductivity, comparison of electrical properties of LCO powders) was investigated. Our studies provide important information on the

mechanism of formation, particle growth, size, shape, and control of these characteristics during synthesis.

Materials and methods

Synthesis of $LiCoO_2$ powders

The high purity of cobalt (II) acetate tetrahydrate ($C_4H_6O_4Co \cdot 4H_2O$, reagent grade), lithium acetate dihydrate ($C_2H_3O_2Li \cdot 2H_2O$, purum p.a, crystallized, 97.0% (NT)) and D-(+)-Glucose ($C_6H_{12}O_6$, ≥ 99.5% (GC), Sigma-Aldrich) were used to synthesize $LiCoO_2$ nanocrystalline powders.

Cobalt and lithium acetate salts were dissolved in a small amount of deionized water separately. Then, the solutions were mixed together and the solution of D-(+)-Glucose was added. The prepared solutions were then evaporated until a gel was obtained. The resulting gel precursor was heated from 450 to 900°C for a few hours in air. The synthesis flowchart is presented in Figure 1.

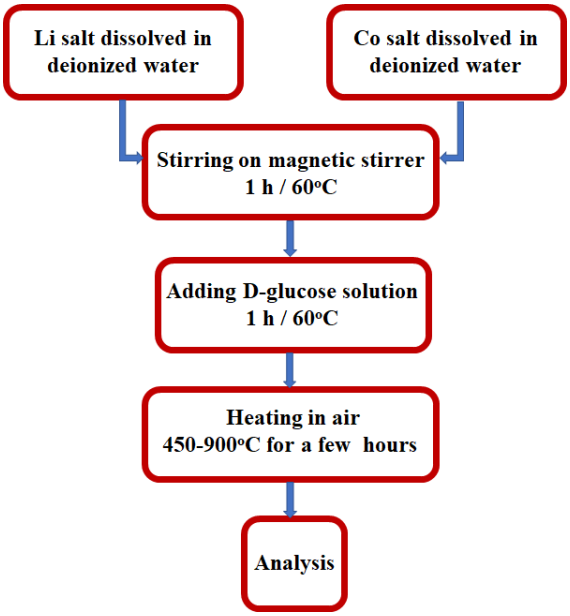

Figure. 1. Flowchart for combustion solution synthesis (CSS) of $LiCoO_2$.

Characterization of $LiCoO_2$ powders

XRD analysis

XRD analysis was performed on a Rigaku Smartlab 3 kW diffractometer equipped with a vertical goniometer. The diffractometer had a Bragg-Brentano (BB) measuring geometry - Θ/2Θ . Radiation: filtered KαCu (λ = 1.5418Å) U=40 kV, I=30 mA. The samples were tested in the angle range 10° - 60°. A measurement step of 0.02^o at a scan rate of 2° / minute was used. A 1D strip detector was used during the analysis: Dtex250.

Specific surface area (SSA) BET

The specific surface area (SSA) of $LiCoO_2$ was determined using the BET nitrogen adsorption isotherm method. The measurements were carried out with the QUADRASORB evo instrument by QUANTACHROME Instruments (USA). Before measurements, the samples were degassed for 5 hours under vacuum. The $LiCoO_2$ was degassed at 200^oC. The purpose of the degassing was to remove impurities from the surface of the tested material. Adsorption measurements were performed with nitrogen at 77 K. For each sample, an analysis was performed at 15 measurement points in the range of $0.05 - 0.3\ P / P_0$ (relative pressure). This is the range of the specific surface area (SSA) study. Above this range, the trend line bends and the averaging of the measurement results is inaccurate, so the result is falsified [62].

Scanning electron microscopy SEM

The morphology of the $LiCoO_2$ crystallites was determined using a scanning electron microscope (SEM) Auriga CrossBeam Workstation (Carl Zeiss). The cross-sections of the fabricated laminates were also observed using this microscope. The SEM images show the morphology of the $LiCoO_2$ obtained at different temperatures, Before analysis, the samples were sputtered by graphite to improve contact. All samples were observed at 1 kV.

EPR analysis

EPR experiments were performed using X-band ELEXSYS E500 (Bruker, Germany) spectrometer. The samples were placed in a Super High Sensitivity Probehead (Bruker, Germany) cavity and in a cryostat where the temperature was determined and stabilized using an Oxford Temperature Controller ITC503S (Oxford Instruments, England). The concentration of paramagnetic ions was obtained using the procedure described elsewhere [60]. Spectral simulations were performed by applying the EasySpin software (version 5.2.27) [61].

Electric properties

The electric properties of the investigated $LiCoO_2$ doped with Mn were studied using the impedance spectroscopy method. For conductivity measurements, pellets of ~1.5 mm thick and 5.15 mm in diameter were prepared from the synthesized material. The powder was pressed at 20 MPa pressure for 1 minute at room temperature. The round surfaces of the samples were covered with silver paste (Hans Wolbring) to form electrodes. The impedance spectroscopy measurements were performed using a Novocontrol AlphaA Broadband Dielectric/Impedance Spectrometer (Novocontrol GmbH) at room temperature. Measurements were carried out in the frequency range from 1 Hz to 1 MHz with an oscillation voltage of 1 V.

Results

XRD analysis

XRD analysis shows that all synthesized $LiCoO_2$ powders from 450 to 900°C (Figure 2) are single phase. All powders have the hexagonal-type $R\bar{3}m$ structure (ICDD PDF card – 50-0653).

As shown in Figure 2, the diffractograms of $LiCoO_2$ powders (*****) heated at different temperatures, from 450°C to 900°C with steps of 50ºC, feature the 7 characteristic

peaks at 2θ angles of 15.2°, 37.3°, 38.9°, 39.0°, 45.4°, 49.7°, 60.0° for CuK_{α} radiation (λ = 1.542 Å), corresponding to the hexagonal (rhombohedral) crystal planes ($R\bar{3}m$ (hkl): (003), (101), (006), (012), (104), (015) and (107), respectively. Phase impurities were not detected by XRD for any of the measured samples. The average size of the crystallites depends on the heating temperature used for the combustion synthesis of powders and lies between 37 and 90 nm (as calculated from the Scherrer formula, allowing for the instrumental line broadening).

Average crystallite sizes, lattice parameters, and cell volumes for all nanocrystalline powders of lithium-cobalt oxide are listed in Table 1. The unit cell parameters and the unit cell volumes of $LiCoO_2$ powders calculated from the XRD data are consistent with the standard values (a_o = 2.81498 Å, c_o = 14.0493 Å, V_0 = 96.41 $Å^3$) of the ICDD PDF card. All the lattice constants are similar to 'ideal' patterns (in the PDF4+2021 ICDD database, the lattice constant for a fixed stoichiometric dispersion pattern is within a: 2.792 – 2.856 Å, c: 14.033 – 14.289 Å) are within the range of the ldata from the literature on the layered structure. The lattice constants depend on the fraction of vacancies and the mixing of Li-Co positions.

There were no significant changes in the lattice constants *a* and *c*, as a function of the temperature and size of the crystallites.

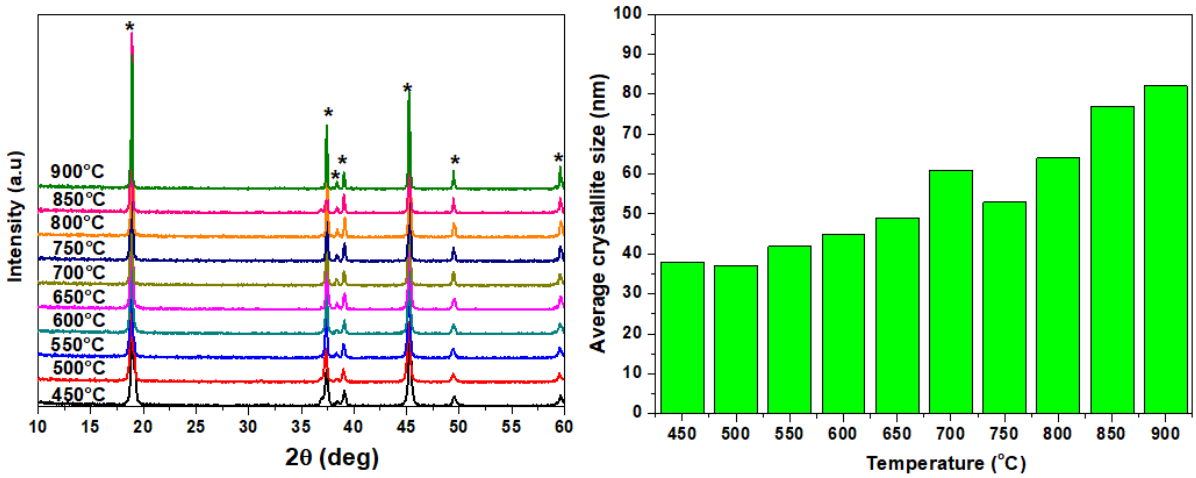

Figure 2: XRD patterns of $LiCoO_2$ heated at different temperatures (450 – 900°C).

Specific surface area SSA (BET)

Table 1 shows the results of the specific surface area (SSA) measurements determined by the Brunauer-Emmett-Teller (BET) adsorption isotherm method. $LiCoO_2$ samples obtained by combustion synthesis were analyzed. From the results obtained, it can be concluded that the value of the specific surface area (SSA) decreases with increasing temperature, and thus the size of the crystallites increases. The highest value was obtained for the sample obtained at 450ºC, while the lowest for the sample obtained at 900ºC. The decrease in the value of the specific surface area (SSA) was approximately 86%. Figure 3 shows the specific surface area (SSA) measurements for $LiCoO_2$ powders as a function of temperature.

Table 1. Lattice parameter, cell volume, average crystalline size (XRD), and specific surface area SSA (BET) for $LiCoO_2$.

Heating temperature [°C]	Average crystalline size [nm]	Lattice parameter a [Å]	Lattice parameter c [Å]	Volume cell V [Å^3]	SSA (BET) [m^2/g]
450	38	2.814	14.040	96.283	3.12
500	37	2.813	14.029	96.134	2.71
550	42	2.814	14.049	96.331	2.46
600	45	2.813	14.044	96.238	2.78
650	49	2.813	14.043	96.246	2.29
700	61	2.815	14.067	96.557	1.67
750	53	2.814	14.060	96.402	0.98
800	64	2.814	14.038	96.275	1.01
850	77	2.814	14.044	96.307	0.47

900	82	2.816	14.058	96.510	0.44

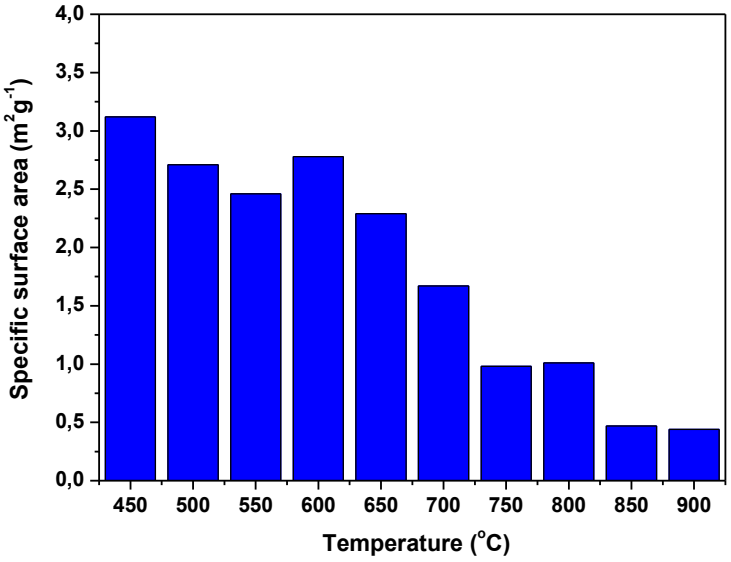

Figure 3. BET and average crystalline size results of LCO powders obtained using combustion solution synthesis.

SEM analysis

Figure 4 shows typical SEM images of all obtained powders. Images were acquired at two magnifications of 10kx and 25kx, respectively.

SEM images show the change in morphology of $LiCoO_2$ samples annealed at different temperatures. It can be seen that as the temperature increases, the morphology changes. Increased temperature results in significant growth in grains. This can be closely correlated with the results of specific grain size and surface area measurements, where changes in these parameters can be seen with increasing temperature (Figure 3). A change in the shape of the crystallites is also evident. A gradual change in the shape and size of the $LiCoO_2$ crystallites can be seen. The higher the temperature, the more regular and less agglomerated powders.

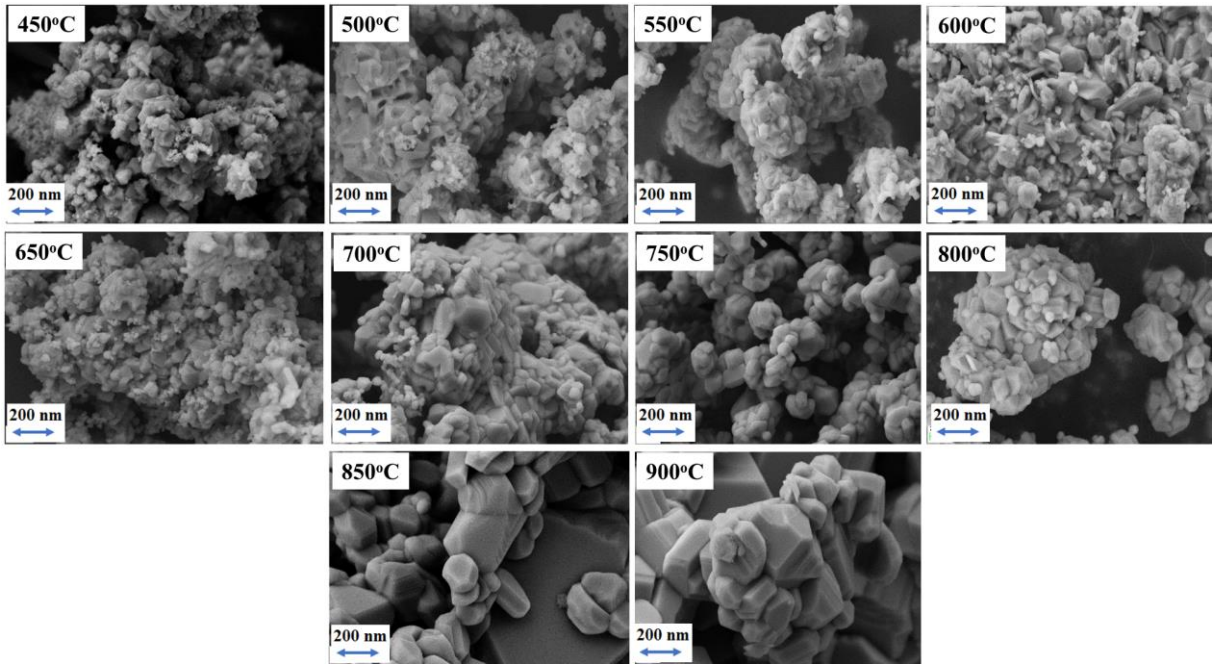

Figure 4. SEM images of $LiCoO_2$ heated at different temperatures (450 – 900°C) at 10x and 25x magnifications.

EPR studies

Electron paramagnetic resonance (EPR) spectra of LCO powders consist at room temperature of a single symmetric line with isotropic g factor 2.142, which indicates isolated Ni^{3+} ions in the crystal structure [63]. The low concentration of Ni^{3+} impurity (35-43 ppm) presented in Figure 5 is almost independent of the synthesis temperature. The exception is the sample heated at 750°C with the lowest impurity concentration on the order of 17 ppm.

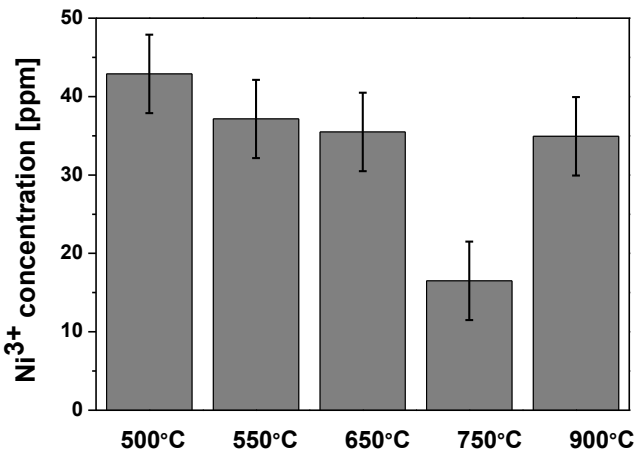

Figure 5. Ni^{3+} impurity concentration depending on the synthesis temperature.

An example of spectral changes in the EPR temperature for the sample synthesized at 900°C is shown in Figure 6. Above about 20 K, a single isotropic line is visible, which is formed from the averaging of the spectroscopic splitting tensor due to the dynamic Jahn-Teller effect. Below about 20 K the dynamic effect becomes a static one, and the spectra show a clear anisotropy due to a static Jahn-Teller distortion.

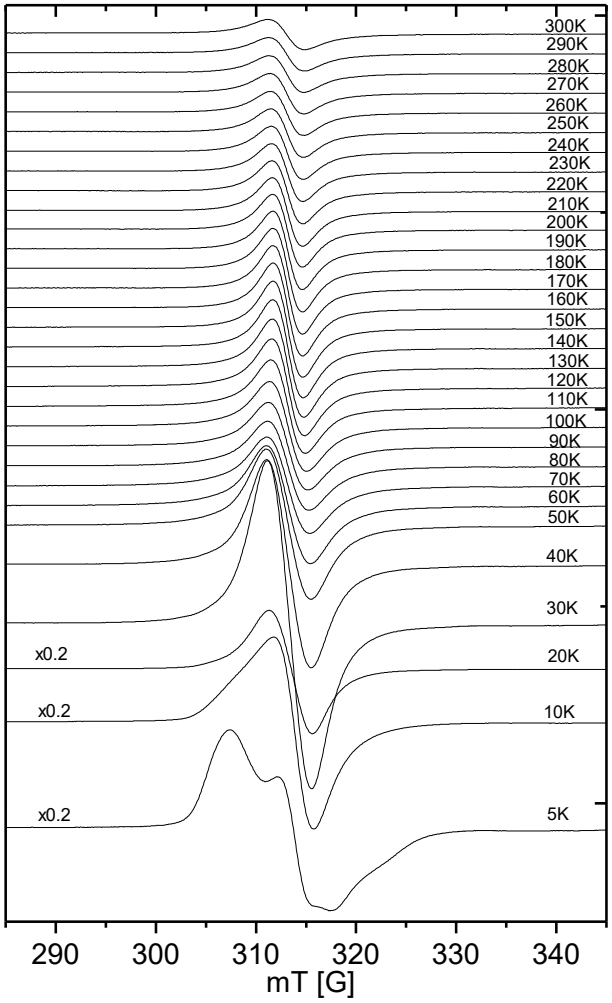

Figure 6. EPR spectra recorded in the temperature range 5-300 K for LCO synthesized at 900°C.

Examples of the experimental spectra simulations obtained at 5 K (Figure 7) show that the EPR spectra for each sample consist of two different nickel complexes. From the simulation of the experimental spectra, we obtained the parameters of the spectroscopic coefficients of tensor g for two Ni^{3+} ions, which are presented in Figure

8. The spin-Hamiltonian parameters indicate that complex Ni(I) has axial symmetry and complex Ni(II) is non-axial.

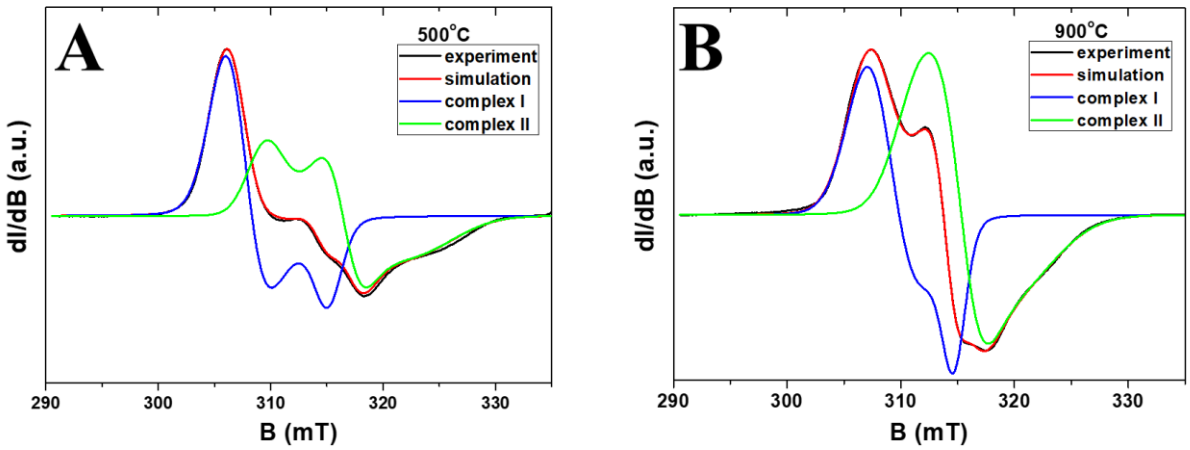

Figure 7. Experimental and simulated spectra for samples prepared at 500°C (a) and 900°C (b) and recorded at 5 K.

The values of the components of the g-tensor (Figure 8) show that the distortion of the coordination environment of Ni^{3+} ions (both axial and non-axial) decreases with the temperature at which the samples were prepared.

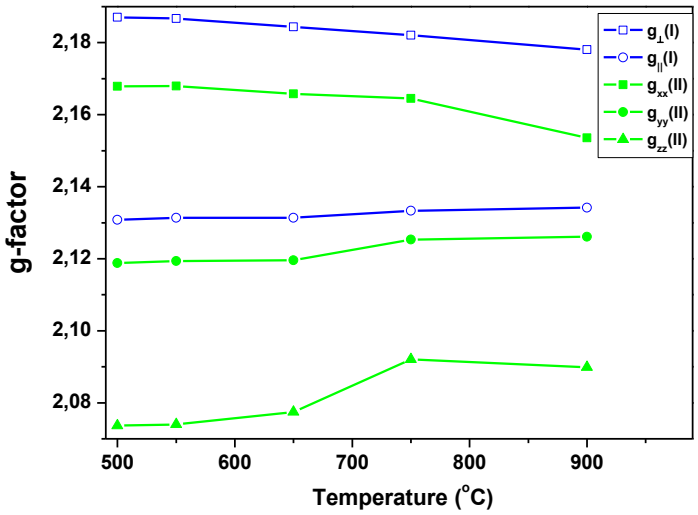

Figure 8. g-tensor components for axial (complex I) and non-axial (complex II) Ni^{3+} ions.

There may be two reasons for the existence of two types of nickel complexes in the spectrum. The first reason may be the expected differences in the g-tensor values

from nickel complexes on the surface and inside the crystallites. However, as shown in Figure 9 the mutual changes in the concentration of Ni^{3+}(I) and Ni^{3+}(II) complexes are too small in relation to the changes in surface area measured by X-ray experiments. Therefore, the assumption that the two different nickel complexes are derived from the crystallites and the surface can probably be rejected.

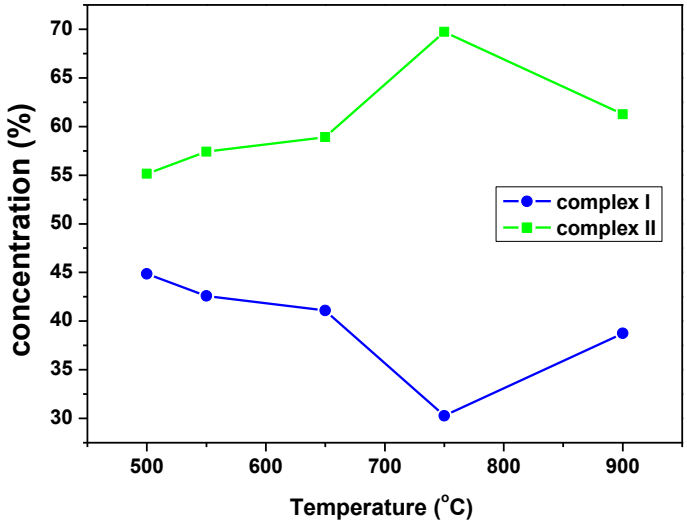

Figure 9. Percentage contribution of Ni^{3+} (I) and Ni^{3+}(II) depending on the sample heating temperature synthesis obtained from the intensity of simulated EPR spectra.

The second reason why two complexes are visible in the EPR spectra is the assumption that two LCO phases are formed during the synthesis: a low-temperature cubic phase (LT-LCO) and a high-temperature trigonal phase (HT-LCO) [64, 65]. In this case, Ni^{3+}(I) in the axial symmetry could be attributed to the cubic phase, and the non-axial complex Ni^{3+}(II) would be characteristic of the trigonal phase. If the nickel admixture is equally well incorporated into both phases, the percentage value of the concentration of individual nickel complexes would also be the percentage value of the individual phases in the tested samples.

Electrical measurements

The electric properties of the investigated $LiCoO_2$ polycrystalline samples were studied using the impedance spectroscopy method. The measurements were

performed for six samples, annealed at selected temperatures: 450°C, 500°C, 550°C, 650°C, 700°C, 750°C, and 900°C. The typical impedance response of the studied materials is presented in Figure 10. It shows the Nyquist's dependence *Z"(Z')* (where *Z'* denotes the real part and *Z"* imaginary part of complex impedance *Z**) of $LiCoO_2$ sample annealed at temperature T=700°C.

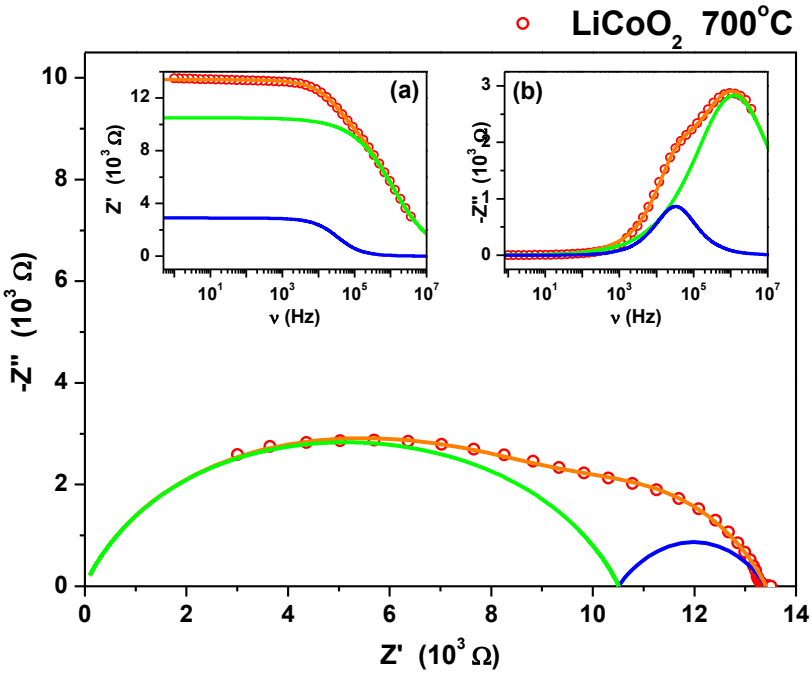

Figure 10. Nyquist plot of $LiCoO_2$ annealed at T=700°C. Insert shows frequency dependences of the real part of impedance Z' and the imaginary part Z" of the studied material. The points represent the measured data, while the orange line shows the calculated total impedance of the sample, the blue line presents fitted data for the grain boundaries, and the green line – fitted date for grain interior (crystalline part of the sample).

The impedance response of the material is presented in Figure 10 and consists of two semicircles. The measured complex *Z** response can be described by connected in series double RC parallel circuit:

$$Z^*(\omega) = \frac{R_1}{1+(i\omega R_1 C_1)^{1-\alpha_1}} + \frac{R_2 - R_1}{1+(i\omega(R_2-R_1)C_2)^{1-\alpha_2}} \quad \textbf{(1)}$$

where: R_1 and R_2 denote the resistance of the first contribution, R_2 is the resistance of the sum of both contributions, C_1 and C_2 denote the electric capacities of the two

circuits, α_1 and α_2 are the parameters, $\omega = 2\pi f$ is the angular frequency of the measuring field *E*-field. Value *α* describes the flattening of the semicircle caused by the distribution of the relaxation time constants. Ideally, when only one time constant describes relaxation processes in the material (Debye-type response), fitting parameter *α* is close to 0 and the flattening of the semicircle is non-existent. The distribution of the time constants is related to the microstructure of the material studied, as the sample is constructed from pressed powder material of different sizes. The response consisting of two semicircles is often observed in polycrystalline samples of ion conductors and ceramics [66, 67] and is related to two different contributions to total conductivity. The two contributions to the total conductivity can be related to the conductivity of the bulk material, crystalline (high-frequency contribution, see insert in Figure 10) and the grain boundaries (low frequency), respectively.

The calculated *R* was used to determine the DC conductivity of the bulk material *σ* using the known sample geometry:

$$\sigma_{dc} = \frac{1}{R}\frac{d}{S}, \qquad \textbf{(2)}$$

where: *d* denotes the thickness and *S* is the surface area of the plane-parallel sample. Table 2 presents a comparison of the DC conductivity of the $LiCoO_2$ samples. A comparison of the influence of the annealing temperature on electrical conductivity shows some very interesting behavior. With increasing temperature of annealing, the value of DC conductivity increases with a maximum temperature of 500°C. For this temperature, the DC conductivity reaches a value of 5.01 10^{-2} S/m. However, an additional increase in the annealing temperature causes a steady decrease in DC conductivity. For the sample of $LiCoO_2$ material annealed at 900°C, the value of DC conductivity is 9.3 10^{-4} S/m. The obtained DC conductivity values are similar to those observed in the literature [68].

Table 2. DC conductivity of the $LiCoO_2$ samples was measured at 293K. Values in the table present only the total conductivity of the sample.

Temperature [°C]	σ_{dc} [10^{-3} S m^{-1}]
450	7.18
500	50.10
550	11.41
650	9.36
700	7.95
750	3.04
900	0.93

Conclusion

Single-phase $LiCoO_2$ powders were prepared using a new combustion synthesis (CS). The influence of temperature heating on structure, morphology, and electrical parameters was analyzed. The XRD results revealed that at the lowest temperature (450°C) the LCO powder was obtained. Furthermore, the average crystallite size (calculated from the Scherrer equation, XRD) increased as well as the grain size (SEM) as the heating temperature increased from 450 to 900°C. A change in the shape of the crystallites is also evident. A gradual change in the shape and size of the $LiCoO_2$ crystallites can be seen. The higher temperature, the more regular and less agglomerated powders were achieved. The specific surface area (SSA) of lithium cobalt oxide powders varies as a function of the heating temperature. From the obtained results, it can be concluded that the value of the specific surface area (SSA) decreases with increasing temperature and thus the size of the crystallites increases. The highest SSA value was obtained for the sample obtained at 450°C, while the lowest value was obtained for the sample obtained at 900°C. Electrical studies showed that conductivity strongly depends on the heating temperature. The samples obtained at the highest temperature had lower (over one magnitude) conductivity. Strong

thermal hysteresis is observed in all samples. However, during cooling, the samples heated to 750°C and 900°C had much higher conductivity.

Acknowledgements

Authors would like to acknowledge Dr. R. Diduszko and Mrs. M. Romaniec (Lukasiewicz Research Network – Institute of Microelectronics and Photonics - IMIF) for XRD and SEM measurements.

ORCID ® iDs

Monika Michalska - https://orcid.org/0000-0002-6120-4950

Paweł Ławniczak - https://orcid.org/0000-0003-1722-5292

Tomasz Strachowski - https://orcid.org/0000-0003-1948-3543

Adam Ostrowski - https://orcid.org/0000-0002-3936-5184

Waldemar Bednarski - https://orcid.org/0000-0003-1956-7501

Funding

This work was financially supported by the Ministry of Education, Youth and Sports, Czech Republic (contract no. 8F21007) through the research project cooperation between the AtomDeC Consortium (V4-Japan/JRP/2021/96/AtomDeC) by funding received from the Visegrad group(V4)-Japan 2021 2nd Joint Call on “Advanced Materials”.

References

1. Mizushima, K. Jones, P. C. Wiseman, P. J. Goodenough J. B., Li_xCoO_2 (0<x<-1): A new cathode material for batteries of high energy density, Materials Research Bulletin 15 ,**1980**, 783-789. https://doi.org/10.1016/0025-5408(80)90012-4

2. Yoshino, A. The Birth of the Lithium-ion Battery, Angewandte Chemie 51 ,**2012**, 5798-5800. https://doi.org/10.1002/anie.201105006

3. Nagaura, T. Tozawa, K. Lithium Ion Rechargeable Battery, Progress in Batteries and Solar Cells 9 ,**1990**, 209-217. Book.

4. Ozawa, K. Lithium-ion rechargeable batteries with $LiCoO_2$ and carbon electrodes: the $LiCoO_2$/C system, Solid State Ionics 69 ,**1994**, 212-221. https://doi.org/10.1016/0167-2738(94)90411-1

5. Shukla, A. K. Kumar, T. P. Materials for next-generation lithium batteries, CURRENT SCIENCE 94 ,**2008**, 314-331.

6. Nitta, N. Wu, F. Lee, J. T. Yushin, G. Li-ion battery materials: present and future, Materials Today 18 ,**2015**, 252-264. https://doi.org/10.1016/j.mattod.2014.10.040

7. Xu, X. Lee, S. Jeong, S. Kim, Y. Cho J. Recent progress on nanostructured 4 V cathode materials for Li-ion batteries for mobile electronics, Materials Today 16 (12),**2013**, 487-495. https://doi.org/10.1016/j.mattod.2013.11.021

8. Nazri, G.-A. Pistoia, G. Lithium Batteries Science and technology, Springer ,**2009**.

9. Fergus J. W. Recent developments in cathode materials for lithium ion batteries, Journal of Power Sources 195 ,**2010**, 939-954. https://doi.org/10.1016/j.jpowsour.2009.08.089

10. Zou, M. Yoshio, M. Gopukumar S., Yamaki J. Synthesis of High-Voltage (4.5 V) Cycling Doped $LiCoO_2$ for Use in Lithium Rechargeable Cells, Chemistry of Materials 15 (25) ,**2003**, 4699-4702. https://doi.org/10.1021/cm0347032

11. Zou, M. Yoshio, M. Gopukumar S., Yamaki J. Performance characteristics of Li//$Li_{1\pm x}CoO_2$ cells, Materials Research Bulletin 40 ,**2005**, 708-714. https://doi.org/10.1016/j.materresbull.2004.12.004

12. Zou, M. Yoshio, M. Gopukumar S., Yamaki J. Performance of $LiM_{0.05}Co_{0.95}O_2$ Cathode Materials in Lithium Rechargeable Cells When Cycled up to 4.5 V, Chemistry of Materials 17 ,**2005**, 1284-1286. https://doi.org/10.1021/cm048734o

13. Sun, Y.-K. Chen, Z. Noh, H.-J. Lee, D.-J. Jung, H.-G. Ren, Y. Wang, S. Yoon, C. S. Myung, S.-T. Amine, K. Nanostructured high-energy cathode materials for advanced lithium batteries, Nature Materials 11 ,**2012**, 942-947. https://doi.org/10.1038/nmat3435

14. Fergus, W. Recent developments in cathode materials for lithium ion batteries, Journal of Power Sources 195 ,**2010**, 939-954. https://doi.org/10.1016/j.jpowsour.2009.08.089

15. Mauger, A. Julien, C. Surface modifications of electrode materials for lithium-ion batteries: status and trends, Ionics 20 ,**2014**, 751-787. https://doi.org/10.1007/s11581-014-1131-2

16. Fu, L. J. Liu, H. Li, C. Wu, Y. P. Rahm, E. Holze, R. Wu, H. Q. Surface modification of electrode materials for lithium ion batteries, Solid State Sciences 8 ,**2006**, 113-128. https://doi.org/10.1016/j.solidstatesciences.2005.10.019

17. Ohzuku, T. Makimura, Y. Layered Lithium Insertion Material of $LiCo_{1/3}Ni_{1/3}Mn_{1/3}O_2$ for Lithium-Ion Batteries, Chemistry Letters 7 ,**2001**, 642-643. https://doi.org/ 10.1246/cl.2001.642

18. Jo, M. Jeong, S. Cho, J. High power $LiCoO_2$ cathode materials with ultra energy density for Li-ion cells, Electrochemistry Communicationas 12 ,**2010**, 992-995. https://doi.org/10.1016/j.elecom.2010.05.010

19. Li, Z. Ban, C. Chernova, N. A. Wu, Z. Upreti, S. Dillon, A. Whittingham, M. S. Towards understanding the rate capability of layered transition metal oxides $LiNi_yMn_yCo_{1-2y}O_2$, Journal of Power Sources 268 ,**2014**, 106-112. https://doi.org/10.1016/j.jpowsour.2014.05.142

20. Needham, S. A. Wang, G. X. Liu, H. K. Drozd, V. A. Liu, R. S. Synthesis and electrochemical performance of doped $LiCoO_2$ materials, Journal of Power Sources 174 (2) ,**2007**, 828-831. https://doi.org/10.1016/j.jpowsour.2007.06.228

21. Adipranoto, D. S. Ishigaki, T. Hoshikawa, A. Iwase, K. Yonemura, M. Mori, K. Kamiyama, T. Morii, Y. Hayashi, M. Neutron diffraction studies on structural effect for Ni-doping in $LiCo_{1-x}Ni_xO_2$, Solid State Ionics 262 ,**2014**, 92-97. https://doi.org/10.1016/j.ssi.2013.11.014

22. Caballero, A. Hernán, L. Morales, J. Castellón, E. R. Santos, J. Enhancing the electrochemical properties of LT-$LiCoO_2$ in lithium cells by doping with Mn, Journal of Power Sources 128 ,**2004**, 286-291. https://doi.org/10.1016/j.jpowsour.2003.09.061

23. Jiang, C. Hosono, E. Zhou, H. Nanomaterials for lithium ion batteries, Nano Today 1 ,**2006**, 28-33. https://doi.org/10.1016/S1748-0132(06)70114-1

24. Lee, K. T. Cho, J. Role of nanosize in lithium reactive nanomaterials for lithium ion batteries, Nano Today 6 ,**2011**, 28-41. https://doi.org/10.1016/j.nantod.2010.11.002

25. Wang, Y. Li, H. He, P. Hosono, E. Zhou, H. Nano active materials for lithium-ion batteries, Nanoscale 2 ,**2010**, 1294-1305. https://doi.org/10.1039/C0NR00068J

26. Michalska, M. Lipińska, L. Sikora, A. Ziółkowska, D. Korona, K. P. Andrzejczuk, M. Structural and morphological studies of manganese-based cathode materials for lithium ion batteries, Journal of Alloys and Compounds 632 ,**2015**, 256-262. https://doi.org/10.1016/j.jallcom.2014.12.266

27. Michalska, M. Hamankiewicz, B. Ziółkowska, D. Krajewski, M. Lipińska, L. Andrzejczuk, M. Czerwiński, A. Influence of $LiMn_2O_4$ modification with CeO_2 on

electrode performance, Electrochimica Acta 136 ,**2014**, 286-291. https://doi.org/10.1016/j.electacta.2014.05.108

28. Krajewski, M. Michalska, M. Hamankiewicz, B. Ziolkowska, D. Korona, K. P. Jasinski, J. B. Kaminska, M. Lipinska, L. Czerwinski, A. $Li_4Ti_5O_{12}$ modified with Ag nanoparticles as an advanced anode material in lithium-ion batteries, Journal of Power Sources 245 ,**2014**, 764-771. https://doi.org/10.1016/j.jpowsour.2013.07.048

29. Hamankiewicz, B. Michalska, M. Krajewski, M. Ziolkowska, D. Lipińska, L. Kamińska, M. Czerwinski, A. The effect of electrode thickness on electrochemical performance of $LiMn_2O_4$ cathode synthesized by modified sol-gel method, Solid State Ionics 262 ,**2014**, 9-13. https://doi.org/10.1016/j.ssi.2013.08.010

30. Jasinski, J. B. Ziolkowska, D. Michalska, M. Lipinska, L. Korona, K. P. Kamińska, M. Novel Graphene Oxide/Manganese Oxide Nanocomposites, RSC Advances 3,**2013**, 22857-22862. https://doi.org/10.1039/C3RA42254B

31. Michalska, M. Lipińska, L. Mirkowska, M. Aksienionek, M. Diduszko, R. Wasiucionek, M. Nanocrystalline lithium-manganese oxide spinels for Li- ion batteries – sol-gel synthesis and characterization of their structure and selected physical properties, Solid State Ionics 188 ,**2011**, 160–164. https://doi.org/10.1016/j.ssi.2010.12.003

32. Fitriani, R. Ovik, B. D. Long, M. C. Barma, M. Riaz, M. F. M. Sabri, S. M. Said, R. Saidur, A review on nanostructures of high-temperature thermoelectric materials for waste heat recovery, Renewable and Sustainable Energy Reviews 64 ,**2016**, 635–659. https://doi.org/10.1016/j.rser.2016.06.035

33. Li, G. Zhang, J. Synthesis of nano-sized lithium cobalt oxide via a sol–gel method, Applied Surface Science 258 ,**2012**, 7612–7616. https://doi.org/10.1016/j.apsusc.2012.04.102

34. Zhu, C. Yang, C. Yang, W.-D. Hsieh, C.-Y. Ysai, H.-M. Chen, Y.-S. High performances of ultrafine and layered $LiCoO_2$ powders for lithium batteries by a novel sol–gel process, Journal of Alloys and Compounds 496 ,**2010**, 703–709. https://doi.org/10.1016/j.allcom.2010.02.178

35. Gao, S. Wei, W. Ma, M. Qi, J. Yang, J. Chu, S. Zhang, J. Guo, L. Sol–gel synthesis and electrochemical properties of c-axis oriented $LiCoO_2$ for lithium-ion batteries, RSC Advances 5 ,**2015**, 51483-51488. https://doi.org/10.1039/C5RA06571B

36. Larcher, D. Delobel, B. Dantras-Laffont, L. Simon, E. Blach, J.-F. Baudrin, E. Formation of Nanometric HT-$LiCoO_2$ by a Precipitation and Aging Process in an Alcoholic Solution, Inorganic Chemistry 49 ,**2010**, 10949–10955. https://doi.org/10.1021/ic101324e

37. Shin Y.H., Koo, S-M. Kim, D.S. Lee, Y-H. Veriansyah, B. Kim, J. Lee, Y-W. Continuous hydrothermal synthesis of HT-$LiCoO_2$ in supercritical water, Journal of Supercritical Fluids 50 ,**2009**, 250–256. https://doi.org/10.1016/j.supflu.2009.06.012

38. Song, S-W. Han, K-S. Yoshimura, M. Effect of 20°–200°C Fabrication Temperature on Microstructure of Hydrothermally Prepared $LiCoO_2$ Films, Journal of Amarican Ceramic Society 83 ,**2000**, 2839-2844. https://doi.org/10.1111/j.1151-2916.2000.tb01641.x

39. Burukhin, A. Brylev, O. Hany, P. Churagulov, B. R. Hydrothermal synthesis of $LiCoO_2$ for lithium rechargeable batteries, Solid State Ionics 151 ,**2002**, 259–263. https://doi.org/10.1016/S0167-2738(02)00721-X

40. Kim, D.Y. Ju, S.H. Kang, Y.C. Fine-sized $LiCoO_2$ particles prepared by spray pyrolysis from polymeric precursor solution, Materials Research Bulletin 42 ,**2007**, 362-370. https://doi.org/10.1016/j.materresbull.2006.05.024

41. Choi, K.Y. Kim, K.D. Yang, J.W. Optimization of the synthesis conditions of $LiCoO_2$ for lithium secondary battery by ultrasonic spray pyrolysis process, Journal of Materials

Processing Technology 171 ,**2006**, 116-124. https://doi.org/ 10.1016/j.jmatprotec.2005.06.060

42. Kondo, A. Nakamura, E. Kozawa, T. Abe, H. Naito, M. Yoshida, J. Nakanishi, S. Iba, H. One-pot mechanical synthesis of the nanocomposite granule of $LiCoO_2$ nanoparticles, Advanced Powder Technology 25 ,**2014**, 1280–1284. https://doi.org/10.1016/j.apt.2014.03.005

43. Xuanye, Y. Hongge, Y. Jihua, C. Mao, H. Feng, X. Zhengfu, Z. Hongmei, X. Solid state synthesis of ultrafine-$LiCoO_2$ by enhanced thermal decomposition of carbonate precursors followed by double-calcining, Solid State Ionics 289 ,**2016**, 159–167. https://doi.org/10.1016/j.ssi.2016.03.005

44. Yan, H. Huang, X. Lu, Z. Huang, H. Xue, R. Chen, L. Microwave synthesis of $LiCoO_2$ cathode materials, Journal of Power Sources 68 ,**1997**, 530-532. https://doi.org/ 10.1016/S0378-7753(96)02565-7

45. Yan, H. Huang, X. Li, H. Chen, L. Electrochemical study on $LiCoO_2$ synthesized by microwave energy, Solid State Ionics 113-115 ,**1998**, 11-15. https://doi.org/ 10.1016/S0167-2738(98)00360-9

46. Subramanian, V. Chen, C. L. Chou, H. S. Fey, G. T. K. Microwave-assisted solid-state synthesis of $LiCoO_2$ and its electrochemical properties as a cathode material for lithium batteries, Journal of Materials Chemistry 11 ,**2001**, 3348-3353. https://doi.org/10.1039/B105008G

47. Gonzalo, E. C. Morán, E. Parada, C. Ehrenberg, H. Microwave-assisted synthesis of $LiCoO_2$ and $LiCo_{1-x}Ga_xO_2$: Structural features, magnetism and electrochemical characterization, Materials Chemistry and Physics 121 ,**2010**, 484–488. https://doi.org/ 10.1016/j.matchemphys.2010.02.011

48. Aruna, S. T. Mukasyan, A. S. Combustion synthesis and nanomaterials, Current Opinion in Solid State and Materials Science 12 ,**2008**, 44-50. https://doi.org/10.1016/j.cossms.2008.12.002

49. Julien, C. 4-Volt Cathode Materials for Rechargeable Lithium Batteries Wet-Chemistry Synthesis, Structure and Electrochemistry, IONICS 6 ,**2000**, 30-46. https://doi.org/10.1007/BF02375545

50. Varna, A. Mukasyan, A. S. Rogachev, A. S. Manukyan, K. V. Solution Combustion Synthesis of Nanoscale Materials, Chemical Reviews 116 ,**2016**, 14493–14586. https://doi.org/10.1021/acs.chemrev.6b00279

51. Mukasyan, A. S. Epstein, P. Dinka, P. Solution combustion synthesis of nanomaterials, Proceedings of the Combustion Institute 31 ,**2007**, 1789-1795. https://doi.org/10.1016/j.proci.2006.07.052

52. Hwang, C.-C. Wu, T.-Y. Wan, J. Tsai, J.-S. Development of a novel combustion synthesis method for synthesizing of ceramic oxide powders, Materials Science and Engineering: B 111 ,**2004**, 49-56. https://doi.org/10.1016/j.mseb.2004.03.023

53. Wen, W. Wu, J.-M. Nanomaterials via solution combustion synthesis: a step nearer to controllability, RSC Advances 4 ,**2014**, 58090-58100. https://doi.org/10.1039/C4RA10145F

54. Li, F.-Y. Ran, J. Jaroniec, M. Qiao, S. Z. Solution combustion synthesis of metal oxide nanomaterials for energy storage and conversion, Nanoscale 7 ,**2015**, 17590-17610. https://doi.org/10.1039/C5NR05299H

55. Vivekanandhan, S. Venkateswarlu, M. Satyanarayana, N. Ammonium carboxylates assisted combustion process for the synthesis of nanocrystalline $LiCoO_2$ powders, Materials Chemistry and Physics 109 ,**2008**, 241–248. https://doi.org/10.1016/j.matchemphys.2007.11.027

56. Santiago, E.I. Andrade, A.V.C. Paiva-Santos, C.O. Bulhoes, L.O.S. Structural and electrochemical properties of $LiCoO_2$ prepared by combustion synthesis, Solid State Ionics 158 ,**2003**, 91–102. https://doi.org/10.1016/S0167-2738(02)00765-8

57. Kalyani, P. Kalaiselvi, N. Mniyandi, N. A new solution combustion route to synthesize $LiCoO_2$ and $LiMn_2O_4$, Journal of Power Sources 111 ,**2002**, 232-238. https://doi.org/10.1016/S0378-7753(02)00307-5

58. Paromita Ghosh, Mahanty, S. Basu, R.N. Effect of silver addition on the properties of combustion synthesized nanocrystalline $LiCoO_2$, Materials Chemistry and Physics 110 ,**2008**, 406–410. https://doi.org/10.1016/j.matchemphys.2008.02.030

59. Rodrigues, S. Munichandraiah, N. Shukla, A.K. Novel solution-combustion synthesis of $LiCoO_2$ and its characterization as cathode material for lithium-ion cells, Journal of Power Sources 102 ,**2001**, 322–325. https://doi.org/10.1016/S0378-7753(01)00770-4

60. Mai, V.C. Bednarski, W. Borowiak-Sobkowiak, B. Wilkaniec, B. Samardakiewicz, S. Morkunas, I. Oxidative stress in pea seedling leaves in response to Acyrthosiphon pisum infestation, Phytochemistry 93 ,**2013**, 49-62.doi.org/10.1016/j.phytochem.2013.02.011

61. Stoll, S. Schweiger, A. EasySpin, a comprehensive software package for spectral simulation and analysis in EPR, Journal of Magnetic Resonance 178 ,**2006**, 42-55 doi.org/10.1016/j.jmr.2005.08.013

62. Strachowski, T. Woluntarski, M. Djas, M. Kowiorski, K. Wiliński, Z. Baran, M. Jagiełło, J. Winkowska, M. Lipińska, L. The influence of reducing agents on the reduced graphene oxide specific surface area determined on the basis of nitrogen adsorption isotherm, Electronics Materials 45 ,**2017**, 2-4.

63. Stoyanova, R. Zhecheva, E. Alcintara, R. Lavelab, P. Tirado, J. L. EPR studies of $Li_{1-x}(Ni_yCo_{1-y})_{1+x}O_2$ solid solutions, Solid State Communications 102 ,**1997**, 457-462. https://doi.org/10.1016/S0038-1098(97)00008-2

64. Antolini, E. $LiCoO_2$: formation, structure, lithium and oxygen nonstoichiometry, electrochemical behaviour and transport properties, Solid State Ionics 170 ,**2004**, 159–171. https://doi.org/10.1016/j.ssi.2004.04.003

65. Han, C.-H. Hong, Y.-S. Park, C. M. Kim, K. Synthesis and electrochemical properties of lithium cobalt oxides prepared by molten-salt synthesis using the eutectic mixture of $LiCl–Li_2CO_3$, Journal of Power Sources 92 ,**2001**, 95-101. https://doi.org/10.1016/S0378-7753(00)00505-X

66. Barsoukov, E. Macdonald, J. R. Impedance Spectroscopy Theory, Experiment, and Applications, Second Eds., J. Wiley&Sons, Inc. Hoboken, New Jersey ,**2005**, 240.

67. Ławniczak, P. Pogorzelec-Glaser, K. Pietraszko, A. Hilczer, B. Effect of disordered imidazole substructure on proton dynamics in imidazolium malonic acid salt, Acta Crystallographica B. 77 ,**2021**, 31-40. https://doi.org/10.1107/S2052520620014365

68. Levasseur, S. Ménétrier, M. Delmas, C. On the Dual Effect of Mg Doping in $LiCoO_2$ and $Li_{1+\delta}CoO_2$: Structural, Electronic Properties, and ^7Li MAS NMR Studies, Chem. Mater. 14 ,**2002**,3584-3590. https://doi.org/10.1021/cm021107j